



Deep circulation in the South China Sea simulated in a regional model

Xiaolong Zhao^{1,2} · Chun Zhou² · Xiaobiao Xu³ · Ruijie Ye^{2,4} · Wei Zhao²

Received: 8 March 2020 / Accepted: 15 September 2020
© Springer-Verlag GmbH Germany, part of Springer Nature 2020

Abstract

In this study, deep circulation in the South China Sea (SCS) is investigated using results from mesoscale-eddy-resolving, regional simulations using the Hybrid Coordinate Ocean Model (HYCOM) verified by continuous current-meter observations. Analysis of these results provides a detailed spatial structure and temporal variability of the deep circulation in the SCS. The major features of the SCS deep circulation are a basin-scale cyclonic gyre and a concentrated deep western boundary current (DWBC). Transport of the DWBC is ~ 2 Sv at 16.5°N with a width of ~ 53 km. Flowing southwestward, the narrow DWBC becomes weaker and wider. The model results reveal the existence of 80- to 120-day oscillation in the deep northeastern circulation and the DWBC, which are also the areas with elevated eddy kinetic energy. This intraseasonal oscillation propagates northwestward with a velocity amplitude of ~ 1.0 to 1.5 cm s^{-1} . The distribution of mixing parameters in the deep SCS plays a role in both spatial structure and volume transport of the deep circulation. Compared with the northern shelf of the SCS and the Luzon Strait, deep circulation in the SCS is more sensitive to the large vertical mixing parameters of the Zhongsha Island Chain area.

Keywords Deep circulation · South China Sea · Spatial structure · Temporal variability · Mixing

1 Introduction

The South China Sea (SCS, Fig. 1) is the largest marginal sea in the Southeast Asian Waters, with an area of approximately 3.5×10^6 km^2 and a depth exceeding 4000 m in the central basin (Wyrski 1961). It is connected to the surrounding waters

mostly by shallow straits: Taiwan Strait to the East China Sea in the north, the Karimata Strait to the Java Sea in the south, and the Mindoro Strait to the Sulu Sea in the southeast. The 355-km-wide Luzon Strait, with a sill depth of ~ 2400 m, is the only deep connection between the SCS and its ambient oceans. There, cold and salty (thus dense) North Pacific Deep Water (NPDW, with potential temperature and salinity of ~ 1.79 $^\circ\text{C}$ and 34.64 psu; Mantyla 1975; Zhao et al. 2016) penetrates the SCS basin through the deepwater overflow in the Luzon Strait driven by the baroclinic pressure gradient between the Pacific Ocean and the SCS (Qu et al. 2006a; Zhao et al. 2014; Zhou et al. 2014, 2018). Since the SCS is closed below 2400 m, the incoming NPDW eventually upwells as a result of enhanced mixing ($\sim 10^{-3}$ $\text{m}^2 \text{s}^{-1}$; Tian et al. 2009; Alford et al. 2011; Yang et al. 2016; Quan and Xue 2019) and exits the SCS either in the intermediate layer through the Luzon Strait back to the Pacific Ocean (Chao et al. 1996; Chen and Huang 1996; Li and Qu 2006; Qu et al. 2000; Tian et al. 2006; Zhang et al. 2015; Gan et al. 2016; Zhu et al. 2019; Cai et al. 2020) or in the upper layer through several shallow straits in the southern part of the SCS to the Java and Sulu Seas (e.g., Qu et al. 2009; Yaremchuk et al. 2009). This three-dimensional circulation, also known as the SCS throughflow (Qu et al. 2006b), serving as a heat and freshwater conveyor that is climatologically important on

Responsible Editor: Fanghua Xu

Electronic supplementary material The online version of this article (<https://doi.org/10.1007/s10236-020-01411-2>) contains supplementary material, which is available to authorized users.

✉ Chun Zhou
chunzhou@ouc.edu.cn

- ¹ North China Sea Marine Forecasting Center, State Oceanic Administration, Qingdao 266061, People's Republic of China
- ² Key Laboratory of Physical Oceanography/CIMST, Ocean University of China and Qingdao National Laboratory for Marine Science and Technology, Qingdao 266100, People's Republic of China
- ³ Center for Ocean-Atmospheric Prediction Studies (COAPS), Florida State University, Tallahassee, FL, USA
- ⁴ State Key Laboratory of Satellite Ocean Environment Dynamics, Second Institute of Oceanography, Ministry of Natural Resources, Hangzhou 310012, People's Republic of China

diffusivity in the SCS and the Luzon Strait increases from about $10^{-3} \text{ m}^2 \text{ s}^{-1}$ at 1000 m to $10^{-2} \text{ m}^2 \text{ s}^{-1}$ near the sea floor. This is about two orders of magnitude higher than that in the North Pacific Ocean and is furnished by energetic internal waves induced by the prominent bathymetry in the Luzon Strait (Niwa and Hibiya 2004; Jan et al. 2007; Tian et al. 2003, 2006). Based on hydrographic measurements with fine-scale parameterizations from 335 stations (477 casts), Yang et al. (2016) recently obtained the three-dimensional distribution of turbulent mixing in the SCS for the first time. Two mixing “hotspots” were identified in the bottom waters in the northern shelf of the SCS and the Luzon Strait and the Zhongsha Island Chain areas (their Fig. 4), largely due to internal tide, bottom bathymetry, and near-inertial energy. Previous studies have shown that enhanced mixing plays a role in deep circulation in both the Pacific Ocean and the Luzon Strait. Furue and Endoh (2005) indicated that the deep Pacific Ocean diffusivity contributes to enhanced production of the Antarctic Bottom Water in the model. The northward transport of the deep meridional overturning circulation across the equator in the Pacific Ocean is stronger with the intense mixing than with weak mixing (Endoh and Hibiya 2006; their Fig. 3). Zhao et al. (2014) suggested that enhanced mixing in the SCS and the Luzon Strait was the primary driving mechanism for the deep circulation in the Luzon Strait, since it is a key process responsible for the density difference between the Pacific Ocean and the SCS. Based on a simulated tidal mixing scheme, Wang et al. (2017) indicated that the tide-induced diapycnal mixing in the Luzon Strait would have a negative effect on driving the cyclonic SCS deep circulation, although without the feature of two mixing “hotspots”. Using a modified four-layer model with parameterizing the mixing effect as the exchange velocity between the middle and deep layers of the SCS, Quan and Xue (2019) suggested that the pattern and evolution of the deep circulation were significantly dependent on the spatiotemporal variability of mixing. Since the mixing is very strong and unevenly distributed in the deep SCS, it is necessary to modify the mixing scheme in the ocean model to be consistent with observed three-dimensional distribution of mixing. Nevertheless, previous numerical studies simulated the deep circulation with homogeneous or simulated vertical mixing parameters in the deep SCS, and one wonders about the sensitivity of the SCS deep circulation to the observed distribution of mixing.

Combining the mooring array in Zhou et al. (2017) with results from mesoscale-eddy-resolving model simulations, the present study for the first time investigates deep circulation under two mixing “hotspots” in the SCS. The paper is organized as follows. After the introduction, the data and model configuration are described in Section 2. Section 3.1 presents the model results compared with observations. Section 3.2 is devoted to the horizontal pattern of mean circulation. Variability of deep

circulation is discussed in Section 3.3, and Section 3.4 examines sensitivity to distribution of mixing. Summary and discussion follow in Section 4.

2 Data and model configuration

As part of the SCS mooring array, an array of six bottom-anchored moorings was deployed off the eastern slope of the Zhongsha Islands between 28 August 2012 and 11 January 2014 (M1-M6, see Fig. 1 for locations). Twenty-nine Aanderaa Data Instruments RCM Seaguard current meters were utilized to measure the horizontal current of the DWBC at nominal depths of 2000 m, 2500 m, 3000 m, 3500 m, and 4000 m, with generally 500 m resolution vertically. Details pertinent to these moorings are shown in Table 1. All current meters were configured to record data at a sample interval of 1 h. Detailed results are discussed in Zhou et al. (2017). Here, we use the observed mean velocity section to examine the simulated time mean structure of the DWBC.

The regional simulation is similar to that of Zhao et al. (2014). The general circulation model used was the Hybrid Coordinate Ocean Model (HYCOM; Bleck 2002; Chassignet et al. 2003) configured with a horizontal resolution of $1/12^\circ$ (~ 9 km resolution in our area of interest). The computational domain, which extends from 4°N to 25°N and 105°E to 125°E (Fig. 1), includes the SCS and part of the northwestern Pacific Ocean. A total of 32 vertical hybrid layers are configured with density referenced to 2000 m (σ_2 , kg m^{-3}): 28.10, 28.90, 29.70, 30.50, 30.95, 31.50, 32.05, 32.60, 33.15, 33.70, 34.25, 34.75, 35.15, 35.50, 35.80, 36.04, 36.20, 36.34, 36.46, 36.56, 36.64, 36.70, 36.74, 36.78, 36.82, 36.84, 36.86, 36.88, 36.92, 36.96, 37.01, and 37.06. The bottom topography is from version 13.1 of Smith and Sandwell (1997) with $1/60^\circ$ resolution. The simulation was initialized with the velocity at rest and January temperature and salinity fields from the third version of monthly $1/4^\circ$ ocean climatology GDEM (Carnes 2009). Since the current work is designed to be a process study, surface forcing was not applied in the experiments. All lateral boundaries were closed with no normal flow, within a 19-grid buffer zone near the eastern boundary, the modeled temperature and salinity are restored toward the monthly climatology from GDEM with an e-folding time of 0.5–32 days that increased with distance from the boundary. The bottom stress was parameterized using a quadratic drag law at the lowest 10 m, with a constant drag coefficient $C_D = 2.5 \times 10^{-3}$.

Based on similar configurations with all of the numerical experiments started from rest and integrated for 10 years, Zhao et al. (2014) studied the deep water circulation in the Luzon Strait, which was in good agreement with the observations based on repeated conductivity-temperature-depth (CTD) and lowered acoustic Doppler current profiler (LADCP) surveys. We modified the K-

Table 1 Mooring configurations with mean zonal and meridional velocities in different depths

Mooring ID	Longitude [°E]	Latitude [°N]	Water depth [m]	Current meter depth [m]	\bar{U} [cm s ⁻¹]	\bar{V} [cm s ⁻¹]
M1	114°35.761'	15°14.855'	3560	1940	-0.47	-0.07
				2440	-1.11	-0.39
				2940	-1.14	-1.08
				3440	-0.58	-0.51
M2	114°42.094'	15°11.961'	4282	2062	-0.15	-0.22
				2562	-0.27	-0.45
				3062	-0.48	-0.76
				3562	-0.64	-1.21
M3	115°07.607'	14°56.235'	4281	2061	0.02	-0.21
				2561	0.22	-0.28
				3061	0.10	-0.40
				3561	-0.30	-0.44
M4	115°20.954'	14°52.977'	4200	4061	-0.27	-0.58
				1980	0.11	0.07
				2480	0.32	0.62
				2980	0.44	0.76
M5	115°51.996'	14°50.133'	4266	3480	0.63	0.53
				3980	0.19	0.39
				2046	-0.53	0.23
				2546	-0.35	0.32
M6	116°03.241'	14°53.750'	4286	3046	-0.30	0.22
				3546	-0.16	0.03
				4046	-0.64	0.24
				2066	-1.33	0.55
				2566	-0.96	0.42
				3066	-1.10	0.02
				3566	-1.39	-0.36
				4066	-1.80	-0.73

profile parameterization (KPP; Large et al. 1994) mixing scheme in accordance with the two observed mixing “hotspots” found in Yang et al. (2016). Thus, the control run was configured with larger vertical mixing parameters, in which the diapycnal diffusivity beneath 1000 m was set to $10^{-3} \text{ m}^2 \text{ s}^{-1}$ in both the northern shelf of the SCS and the Luzon Strait (109–122°E, 18–23°N) and the Zhongsha Island Chain area (109–122°E, 14–17°N, red boxes in Fig. 1). To examine the impact of mixing, four sensitivity experiments were used with the same configuration as the control run, but with different mixing schemes: following Zhao et al. (2014), Exp-5 and Exp-3 were configured with the native KPP scheme as background mixing of $10^{-5} \text{ m}^2 \text{ s}^{-1}$ and the diapycnal diffusivity beneath 1000 m in the SCS and the Luzon Strait (west of 122°E) as $10^{-3} \text{ m}^2 \text{ s}^{-1}$, respectively. Exp-3A and Exp-3C were configured with the larger vertical mixing

parameters in different areas, in which the diapycnal diffusivity beneath 1000 m was set to $10^{-3} \text{ m}^2 \text{ s}^{-1}$ in the northern shelf of the SCS and the Luzon Strait (109–122°E, 18–23°N) and the Zhongsha Island Chain area (109–122°E, 14–17°N), respectively (Table 2). Instead of applying the exact results of mixing distribution of Yang et al. (2016), these configurations are idealized to some extent, in order to reproduce the two mixing “hotspots” dynamically explained by dissipation of internal tides, while not following the specific distribution and magnitude which still need to be verified due to the limitations of numbers of CTD profiles and parameterization method. These configurations may somehow introduce uncertainty to the simulation results which is difficult to evaluate with the current observations.

In order to obtain a steady state of the deep circulation in the SCS, we integrated all of the numerical experiments for

Table 2 Experiment configurations with different mixing schemes. Note that the background mixing of all experiments was set to $10^{-5} \text{ m}^2 \text{ s}^{-1}$

Experiments	Larger vertical mixing parameter areas (diapycnal diffusivity beneath 1000 m set to $10^{-3} \text{ m}^2 \text{ s}^{-1}$)	Latitude and longitude range
Control run	Northern shelf of the SCS and the Luzon Strait Zhongsha Island Chain area	109–122°E, 18–23°N 109–122°E, 14–17°N
Exp-5	None	None
Exp-3	The SCS and the Luzon Strait	west of 122°E
Exp-3A	The northern shelf of the SCS and the Luzon Strait	109–122°E, 18–23°N
Exp-3C	Zhongsha Island Chain area	109–122°E, 14–17°N

20 years and averaged the last 5 years as the simulated annual mean results mentioned below (as shown in Fig. 2, the thickness structure was basically stable in the last 5 years that indicated that the control run has been stable).

3 Key results

Observations from six moorings allow us to examine the simulated time mean structure of the DWBC and results from mesoscale-eddy-resolving model simulations are used to further investigate the structure and mechanisms of the deep circulation in the SCS.

3.1 DWBC in the SCS

Figure 3 presents a comparison between the observed and simulated section view of the mean current in the deep western boundary of the SCS. Considering that the DWBC is constraint by the northeast-southwest shelf, following Zhou et al. (2017), the observed current is re-coordinated into the cross-section (defined as vertical to the section of M1-M4) component and along-section component, with the former generally following the isobaths with positive direction pointing to the southwest. Observations at M5 and M6 are projected to the section (M1–M4). The simulated time-mean structure of velocity shown in Fig. 1 is a zonal section view of 15.4°N for the control run close to these six moorings.

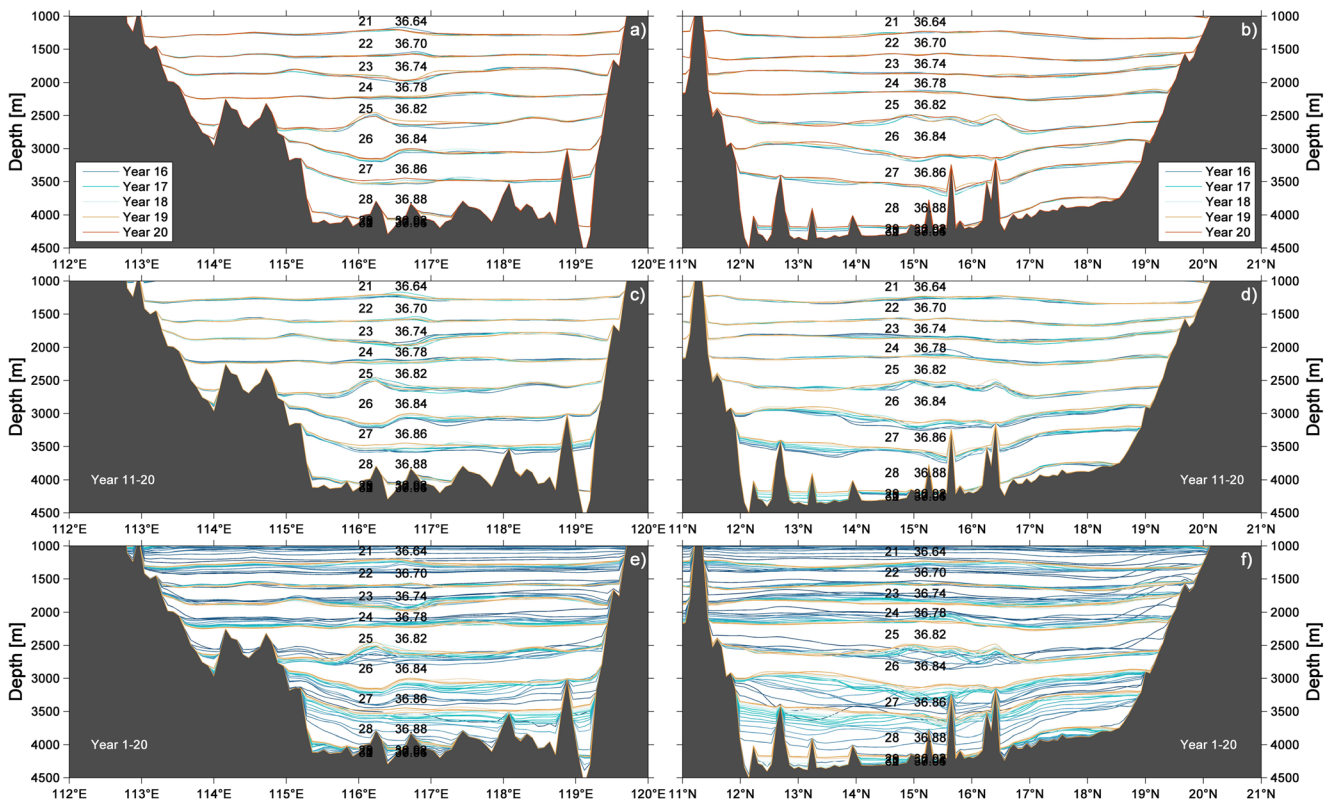
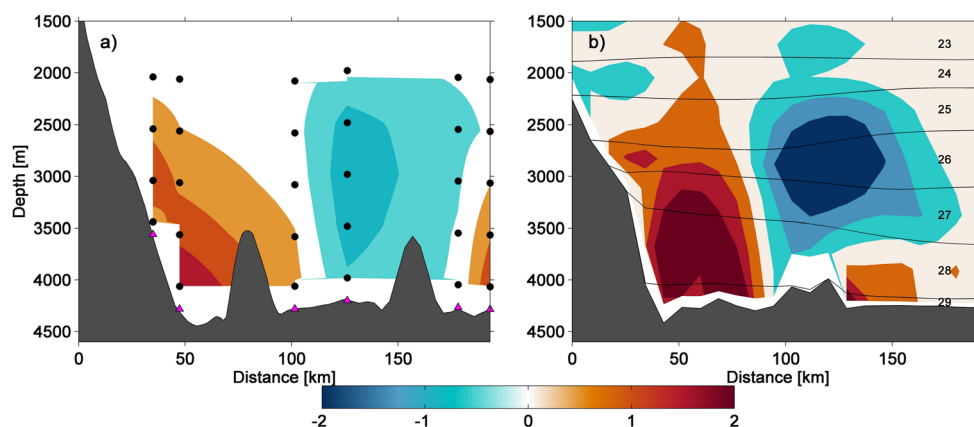


Fig. 2 Section view of year-mean thickness structure at a zonal section of 16.5°N (a, c, e) and a meridional section of 116°E (b, d, f) for the control run. Thickness numbers and density referenced to 2000 m ($\sigma_2, \text{ kg m}^{-3}$) are indicated

Fig. 3 **a** Section view of observed mean cross-section velocity (in cm s^{-1}) from Zhou et al. (2017; their Fig. 2a). Mooring locations are indicated in magenta triangles. Locations of current meters are indicated by black dots. **b** Time-mean structure of velocity (in cm s^{-1}) and thickness numbers at a zonal section of 15.4°N for the control run. Note the positive value represents southward velocity



Consistent with the observations, a bottom intensified current is simulated flowing southwestward off the eastern slope of the Zhongsha Islands. This is different from Lan et al. (2013, 2015) but similar with Shu et al. (2014) and Xu and Oey (2014). It appears that a horizontal resolution of 0.5° is not sufficient to resolve the deep Luzon Strait accurately, resulting in an inaccurate position of the DWBC in the simulation. The DWBC weakens upward, with its upper interface lying at around 2000 m. Horizontally, the model accurately reproduces the observed main axis of the DWBC (comparable with M1 and M2) and a recirculation (comparable with M4 and M5). The DWBC is ~ 100 km wide, with its core leaning on the slope of Zhongsha island. This modeled and observed DWBC is significantly narrower than Wang et al. (2011). Note that the simulated DWBC (4 cm s^{-1}) and recirculation are stronger than the observations (2 cm s^{-1}) since the source, deepwater overflow in the Luzon Strait, is the same status (1.2 to 0.8 Sv; Zhou et al. 2014; Zhao et al. 2016). As expected, the control run shows reasonable agreement with the cross-section observations.

3.2 Mean circulation pattern

To examine the simulated large-scale deep circulation in the SCS, we calculated the mean transports across four zonal sections (13.5°N , 15.0°N , 16.5°N , and 18.0°N) of each layer from the 25th to 30th from 110°E to 121°E (Fig. 4) for the control run. The cumulated transport of the 27th ($\sigma_2 = 36.86 \text{ kg m}^{-3}$, $\sim 3000\text{--}3500$ m) layer shows a northward current in the southern part of the western boundary (near 114°E in sections of 13.5°N and 15.0°N) that belongs to the anti-cyclonic middle layer of the SCS circulation (e.g., Gan et al. 2016; Shu et al. 2014; Xu and Oey 2014; Cai and Gan 2019; Zhu et al. 2019; Cai et al. 2020), while the 28th ($\sigma_2 = 36.88 \text{ kg m}^{-3}$, $\sim 3500\text{--}4000$ m) and 29th ($\sigma_2 = 36.92 \text{ kg m}^{-3}$, $\sim 4000\text{--}4200$ m) layers show a consistent southward DWBC at different latitudes. The mean transport per unit width (in $\text{m}^2 \text{ s}^{-1}$) from the 28th layer shows a strong deep cyclonic circulation in the SCS (Fig. E1a), and the 29th

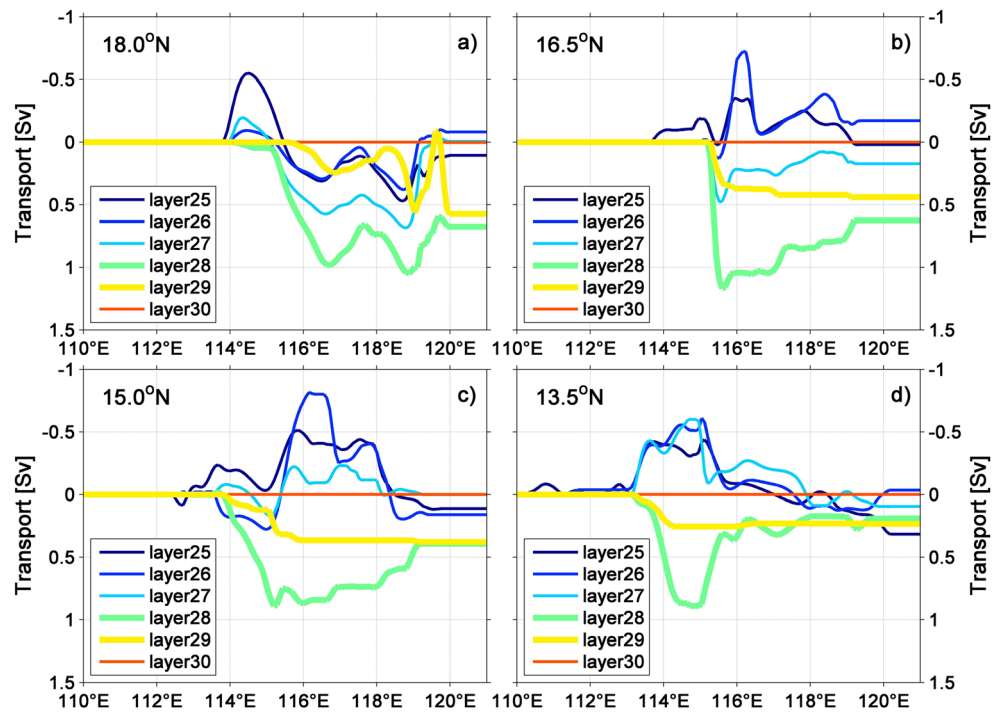
layer mostly presents the deep circulation in the Luzon Strait (Fig. E1b). Therefore, here, we calculate the total mean transport per unit width of the 28th and 29th layers to describe the pathway of deep circulation in the SCS (Fig. 5).

The major features of the SCS deep circulation are a basin-scale cyclonic gyre and a western intensification. Driven by the baroclinic pressure gradient between the Pacific Ocean and the SCS in the Luzon Strait, deepwater overflow spills into the SCS mostly through two gaps in the Heng-Chun Ridge (as WG2 and WG3 in Zhao et al. 2014) along the 3800 m and 4000 m isobaths, respectively. With a confluence off the northern shelf, the current flows southwestward and then turns southward near 116°E , 18°N as an intensified DWBC along the eastern slope of the Zhongsha Islands. Restricted by the topography, the DWBC divides into two branches at 115°E , 15.5°N . A strong southwestward branch follows the western boundary southwestward and another goes southeastward near M4. The rest of the DWBC travels to the deep basin in the south and then turns northeastward into the middle basin, presenting a cyclonic pattern that makes the inflow water spread to nearly the entire SCS deep basin. We cumulated the mean transports across these four zonal sections from different layers to the 29th in order to quantitatively describe the deep circulation in the SCS (Fig. 6). The volume transport of the DWBC is ~ 2.0 Sv at 16.5°N (from the 27th to 29th layers) with a width of ~ 53 km, in agreement with the observed transport (1.65 Sv) and larger than the deepwater overflow in the Luzon Strait (1.2 Sv), which may be related to the entrainment of water from the interior ocean due to enhanced diapycnal mixing in the northeastern SCS (Tian et al. 2009; Yang et al. 2016). While flowing southwestward with an upwelling process, the DWBC becomes weaker and wider: transport of the DWBC becomes ~ 1.2 Sv (from the 28th to 29th layers) with a width of ~ 140 km at 13.5°N .

3.3 Intraseasonal variability of the deep circulation

The model results reveal the existence of energetic intraseasonal variability in the SCS deep circulation. As

Fig. 4 Eastward cumulated of the meridional volume transports (in Sv) across the model section across 4 zonal sections (13.5°N, 15.0°N, 16.5°N, and 18.0°N) of each layer from the 25th to 30th from 110°E to 121°E for the control run. The positive value represents southward volume transport. The depth of the isopycnic interfaces is indicated in Fig. 2b



shown in Fig. 7a, large eddy kinetic energy (EKE, defined as $0.5 \times [(u-\bar{u})^2 + (v-\bar{v})^2]$, where u and v are the zonal and meridional velocities, respectively) areas appear in the deep northeastern circulation and the DWBC, indicating strong variability there. Topography, standing meanders, nonlocal

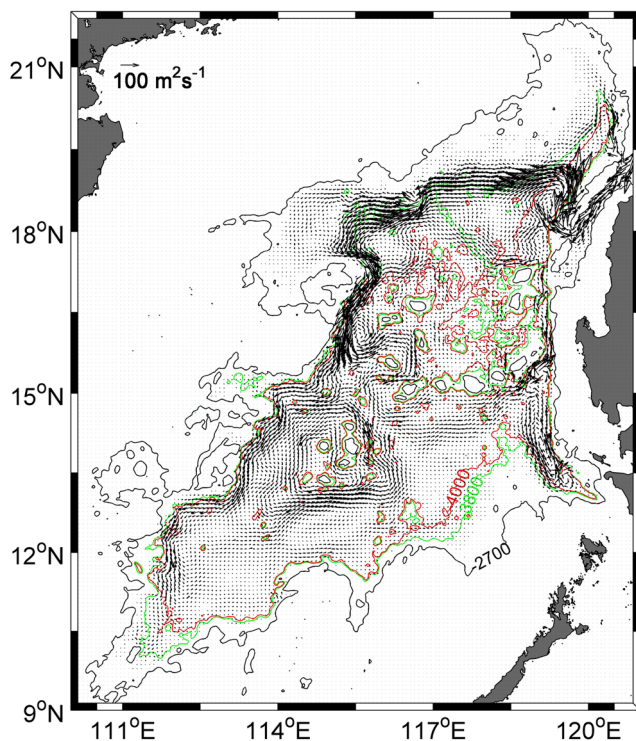
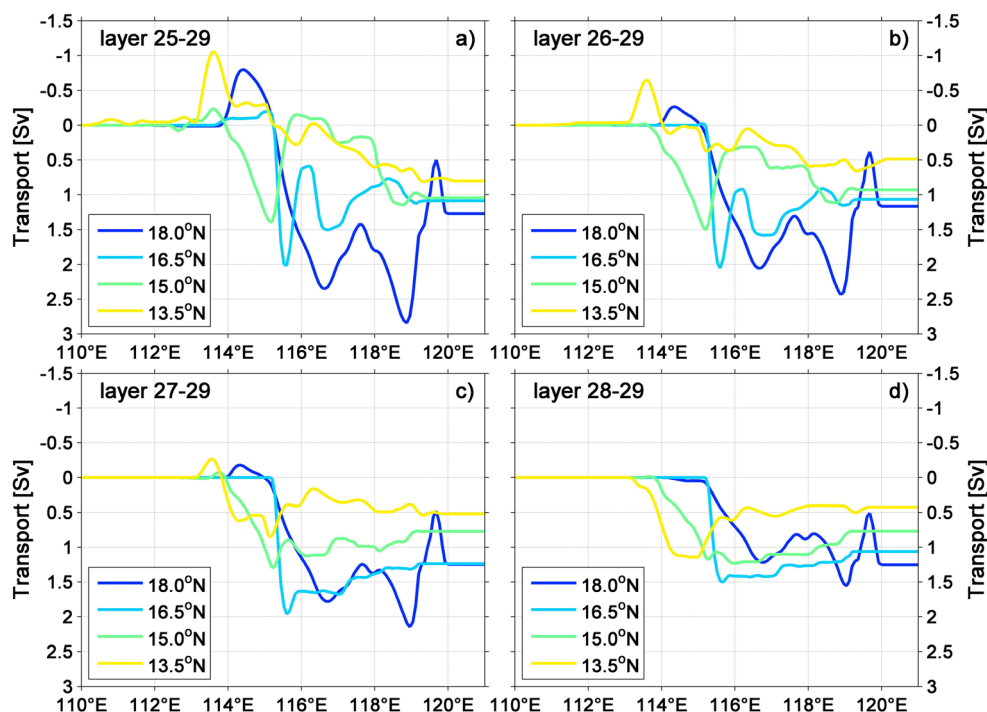


Fig. 5 Total mean volume transport per unit width (in $m^2 s^{-1}$) of the 28th and 29th layers for the control run

energy propagation, and turbulent energy cascade can intricately influence the EKE patterns (e.g., Su and Ingersoll 2016). Periods of max power spectra density (PSD) indicate the dominant feature of the variability at the large EKE areas is an 80- to 120-day oscillation, based on spectrum analyze of zonal and meridional velocity time series from the 28th to 29th layers at each grid point for the control run (Fig. 8). This oscillation also presents in the time series recorded by the six current-meter moorings M1-M6 deployed off the eastern slope of the Zhongsha Islands (Zhou et al. 2017). The relative leading time between the two closed cells in zonal direction can be obtained by calculating the lag correlation of these two zonal velocity time series. And lag correlation analysis is also conducted in meridional direction. Dividing the corresponding distance, we obtain the mean phase speed and direction of the deep oscillation (Fig. 7b). The waves show a northwestward propagation in both the deep northeastern circulation and the DWBC, with a velocity amplitude of ~ 1.0 to $1.5 cm s^{-1}$ (Fig. 7b), comparable with the mean speed of $\sim 2.9 cm s^{-1}$ along the section M1-M6 (Zhou et al. 2017). Based on the principle axis variance ellipse of band-passed velocity and propagation direction, Zhou et al. (2017) suggested that the 80- to 120-day oscillation cannot be attributed to topographic Rossby waves, a mechanism for abyssal intraseasonal variability, especially at the deep western boundary (e.g., Thompson 1977; Johns and Watts 1986; Pickart and Watts 1990; Hamilton 2009). Other possibilities include the barotropic and baroclinic Rossby waves. In another sensitivity experiment, we doubled the SCS basin and the 80- to 120-day oscillation peak disappeared, indicating this oscillation maybe

Fig. 6 Eastward cumulated of the meridional volume transports (in Sv) across the model section across 4 zonal sections (13.5°N, 15.0°N, 16.5°N, and 18.0°N) from different layers to 29th from 110°E to 121°E for the control run. The positive value represents southward volume transport



related to the basin mode of the SCS (e.g., Platzman 1972; Xu et al. 2007). This variability is a good topic for future studies.

3.4 Model sensitivity to distribution of mixing

Exp-5, Exp-3, Exp-3A, and Exp-3C all show a basin-scale cyclonic gyre with a western intensification in the deep SCS (Fig. 9). However, the volume transport of the deepwater overflow in the Luzon Strait, the DWBC, and the detail structure of the deep circulation are quite different in these

experiments. The simulated deep circulation is much weaker in Exp-5 and Exp-3A (e.g., 0.9 and 1.0 Sv is smaller than the control run (1.2 Sv) of the overflow; 1.0 and 0.7 Sv are nearly two times smaller than the control run (2 Sv) at 16.5°N of the DWBC). On the other hand, it is closer to the control run in the Exp-3 and Exp-3C (1.4 and 1.2 Sv of the overflow; 2.2 and 1.9 Sv of the DWBC). Magnitude of upwelling is similar case: the upwelling transports southward from 16.5°N in Exp-5 and Exp-3A (0.6 and 0.6 Sv), two times smaller than the control run (1.2 Sv), while the control run, Exp-3 and Exp-3C are in

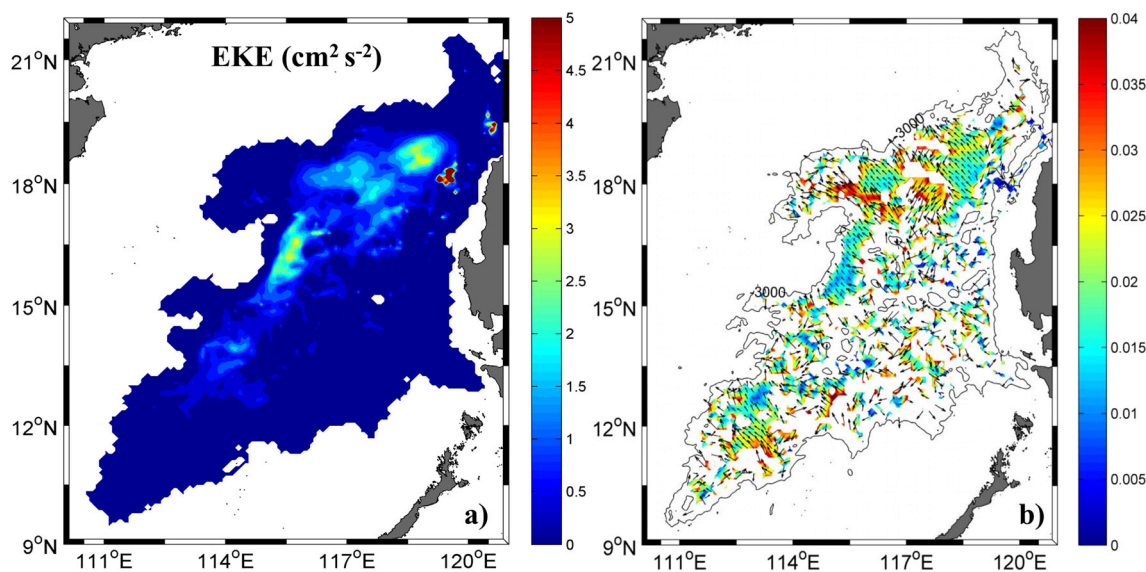


Fig. 7 Distribution of modeled eddy kinetic energy EKE (a, in $\text{cm}^2 \text{s}^{-2}$) in the South China Sea, mean phase speed and direction of propagation (b, in m s^{-1}) from the 28th to 29th layer for the control run

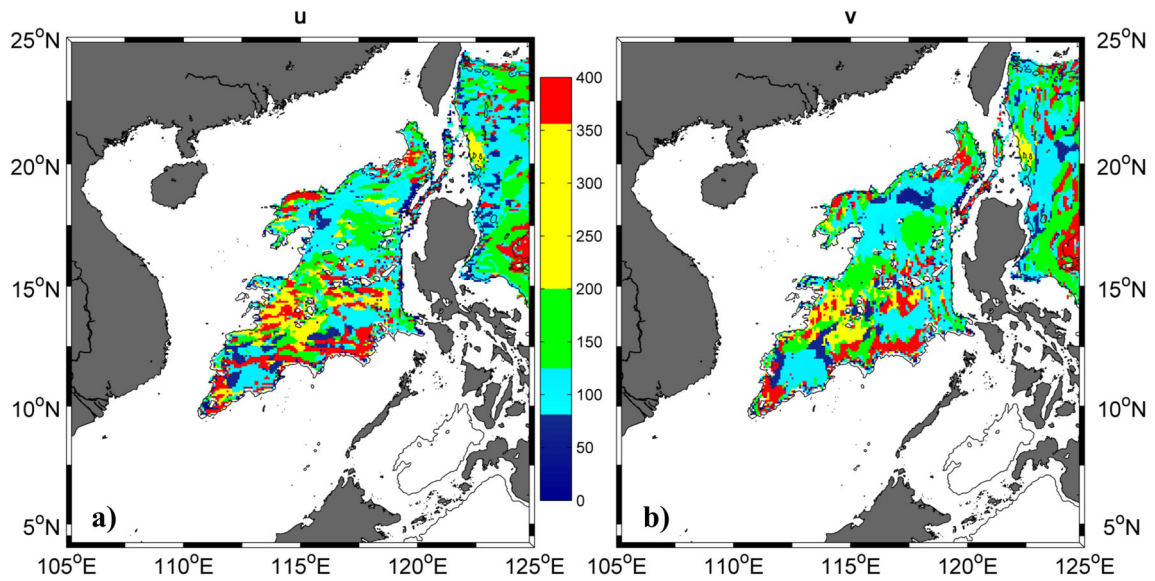


Fig. 8 Periods (in days) of max power spectra density (PSD) of zonal (a) and meridional (b) velocity from the 28th to 29th layer at each grid point for the control run

reasonable agreement (1.2, 1.3, and 1.1 Sv). This indicates that compared with the northern shelf of the SCS and the Luzon Strait, deep circulation in the SCS is more sensitive

to the large vertical mixing parameters of the Zhongsha Island Chain area. This might be explained by the fact that the latter contains more notable density difference due to the

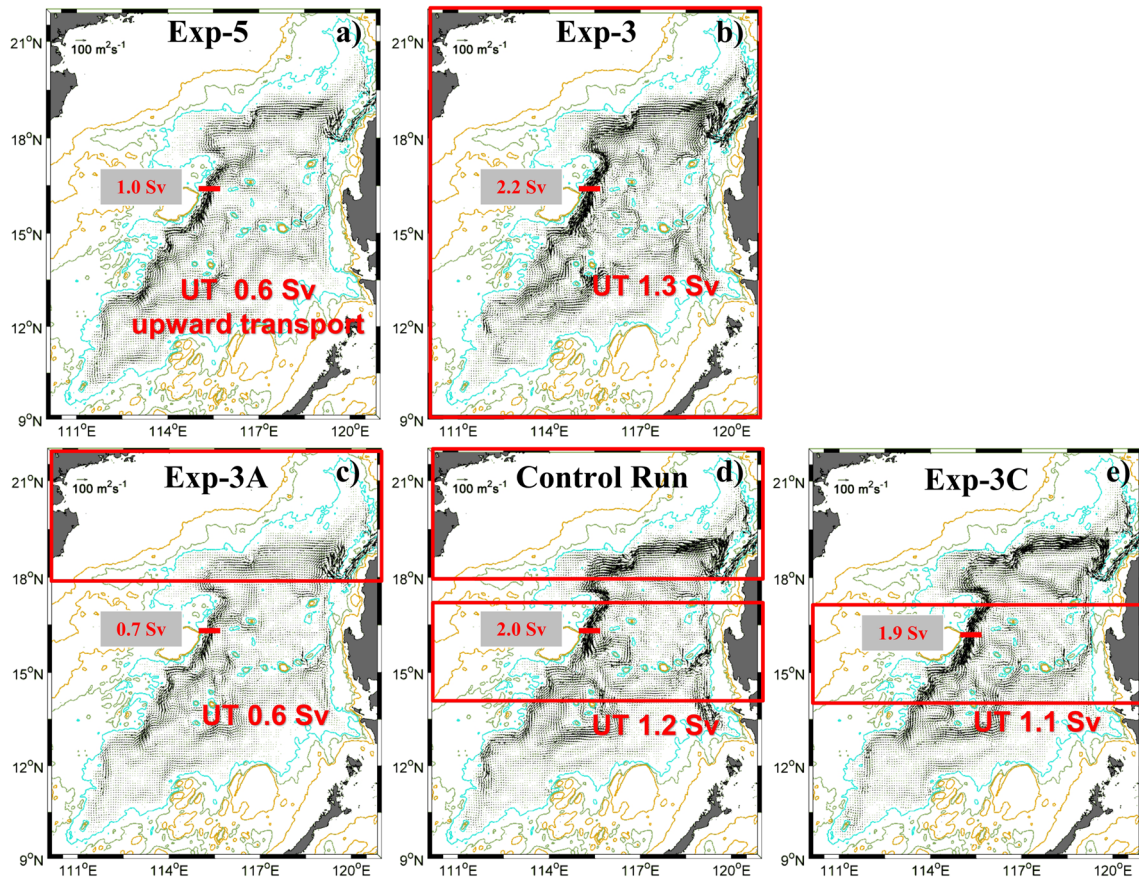


Fig. 9 Total mean volume transport per unit width (in $m^2 s^{-1}$) of the 28th and 29th layers in Exp-5, Exp-3, Exp-3A, control run, and Exp-3C. The cross sections are indicated by red lines and the corresponding volume

transports (in Sv) are indicated in the textboxes with gray background. Red boxes indicate the areas with strong mixing

larger area of enhanced mixing, as the deep circulation is essentially density driven. With an increase in the range of strong mixing, the intensity of the deep circulation in the SCS is enhanced, suggesting that enhanced mixing plays an important role in maintaining the intensity of the SCS deep circulation. At the same time, the spatial structure of the deep circulation in the SCS also changes with different distribution of mixing, which is consistent with the finding of Quan and Xue (2019) based on calculating the entrainment using three methods to parameterize the different abyssal mixing. For example, the southwest sub basin circulation is expanded in Exp-5, while the recirculation near the DWBC extends to the Zhongsha Island Chain area in the control run but not in the other four experiments. By adjusting the thermohaline structure (Fig. 10), enhanced mixing not only impacts the local deep circulation, but can also influence the deep circulation in other areas without enhanced mixing.

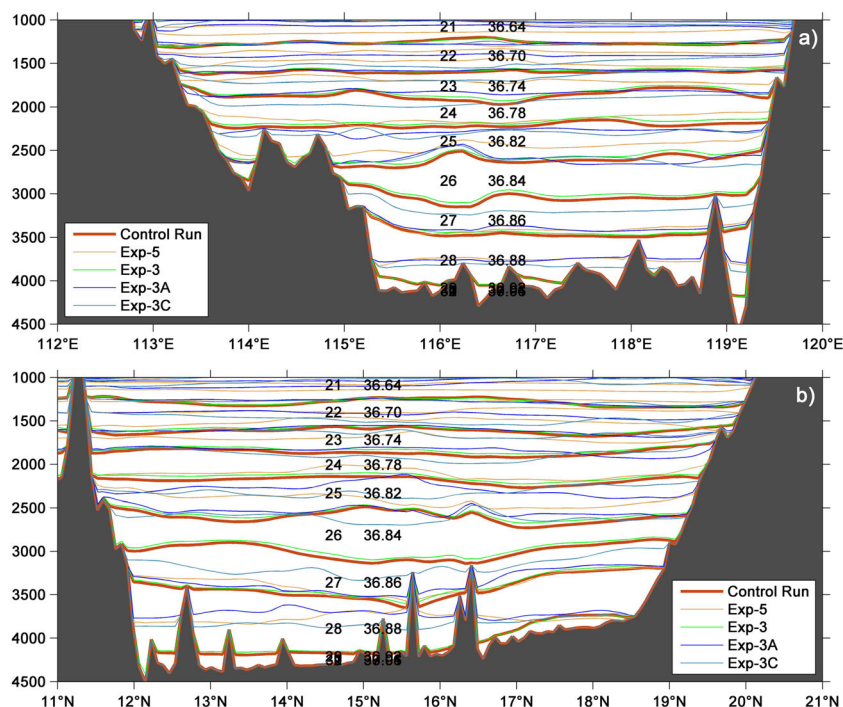
4 Summary and discussion

Due to enhanced mixing in the deep SCS, the deep water in the SCS is expected to move upward much faster than deep water in the open ocean (on the order of 0.1 cm day^{-1} ; e.g., Kunze et al. 2006). Qu et al. (2006a) gave an estimate of area-averaged vertical upwelling velocity of the deepwater in the SCS at $\omega = Q/A = 0.24 \text{ m day}^{-1}$, and applied a hydraulic theory to estimate the Luzon Strait transport $Q = 2.5 \text{ Sv}$ and the area of the SCS at 2000 m to estimate as $A = 9 \times 10^{11} \text{ m}^2$. Based on long-term mooring observations, the upwelling

velocity becomes 0.08 m day^{-1} while $Q = 0.8 \text{ Sv}$ (Zhou et al. 2014; Zhao et al. 2016) in this way. Yang et al. (2016) obtained the vertical velocity as 0.32 m day^{-1} from a vertical advective-diffusive balance model based on the diffusivity results inferred from the Gregg-Henyey-Polzin parameterization and 0.28 m day^{-1} from a dynamically and kinematically consistent ocean state estimate system (Estimating the Circulation and Climate of the Ocean, ECCO; Forget et al. 2015). For the horizontal distribution of upwelling in the deep SCS basin, albeit without estimating the magnitude, Shu et al. (2014) indicated that there are three northwest-southeast tilted zones where tracers upwell inferred from the modeled trajectories. These correspond to the three deep meridional overturning circulation cells. They speculated that one possible mechanism for these upwelling zones is the interaction between the topographically trapped waves on the slope and the westward planetary Rossby waves (e.g., Rhines 1970; Anderson and Gill 1975).

As described in Fig. 6d, the net transport of the 28th and 29th layers at these four sections is all southward, with the values decreasing as 1.25, 1.06, 0.77, and 0.42 Sv , respectively. This indicates that the deep flow goes upward from the deep layer as a result of enhanced mixing in the deep SCS. By dividing the differences between the net transports with corresponding areas, the upward transports are found to be 0.19, 0.29, 0.35, and 0.42 Sv , which indicate that the values of upwelling at each area are 0.19, 0.32, 0.27, and 0.22 m day^{-1} , respectively. We also cumulated the mean transports across four meridional sections (1.15 Sv at 118.5°E , 0.88 Sv at 117.0°E , 0.65 Sv at 115.5°E , and 0.29 Sv at 114.0°E) and the corresponding

Fig. 10 Section view of mean thickness structure at a zonal section of 16.5°N (a) and a meridional section of 116°E (b) for the control run, Exp-5, Exp-3, Exp-3A, and Exp-3C. Thickness numbers and density referenced to 2000 m ($\sigma_2, \text{ kg m}^{-3}$) are indicated



upwelling became 0.28, 0.23, 0.36, and 0.29 m day^{-1} , respectively. This suggests that the DWBC is the strongest upwelling area. Divided the thickness depth difference between the beginning and the end of the last 5 years by the time, we calculated the change of volume above the upper interface of the 28th layer over time as $\sim 0.003 \text{ m day}^{-1}$ ($\sim 2\%$ of the diapycnal velocity of 0.2–0.3 m day^{-1}), which is typically small term. In order to present the horizontal distribution and magnitude of upwelling, we calculated the diapycnal velocity across the upper interface of the 28th layer for the control run in each $1^\circ \times 1^\circ$ box (Fig. 11). The results show that the diapycnal velocity is not uniformly upward (toward lighter water) or downward (toward denser water). The upward transformation takes place around the DWBC and seamounts areas with elevated values of 1 m day^{-1} or larger, whereas the downward transformation (with slightly lower with values of 0.5 m day^{-1}) takes place in the relatively flat inner basin offshore of the DWBC. This diapycnal transformation is due to interior mixing prescribed in the model, and similar complex patterns of upward and downward diapycnal transformation can be found in the upper subpolar North Atlantic Ocean (Xu et al. 2018), where the Labrador Sea Water are formed. The magnitude of net diapycnal transformation in the SCS is close to the input of the deepwater overflow in the Luzon Strait, further implying that the model temperature, salinity, and density drift is small (see Fig. 2 for the displacement of density interface in the last 5 years). In the real ocean, the upwelling near the deep west boundary and seamounts may also be driven by enhanced near-boundary mixing (e.g., Ferrari et al. 2016; McDougall and Ferrari 2017).

In the present study, the deep circulation in the SCS is investigated by mesoscale-eddy-resolving model simulations and found to be in reasonable agreement with mooring arrays.

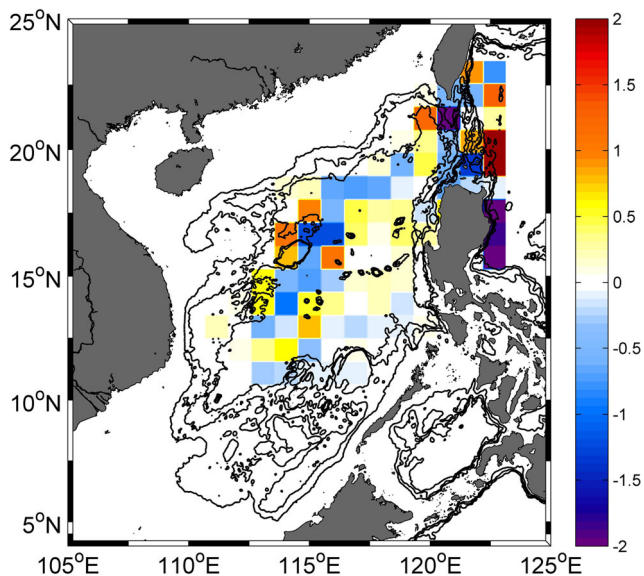


Fig. 11 Horizontal distribution of diapycnal velocity (in m day^{-1}) binned in $1^\circ \times 1^\circ$ cells across upper interface of the 28th layer for the control run

Analysis of these results provides a detailed structure and variability of the deep circulation in the SCS. The major features of the SCS deep circulation are a basin-scale cyclonic gyre and a western intensification. The transport of the DWBC is $\sim 2 \text{ Sv}$ at 16.5°N with a width of $\sim 53 \text{ km}$. Flowing southwestward, the DWBC becomes weaker and wider. By dividing the differences between transports with corresponding areas, the values of upwelling are from 0.19 to 0.36 m day^{-1} , with the strongest area being around the DWBC. The model results reveal the existence of an 80- to 120-day oscillation in the deep northeastern circulation and the DWBC, which are also the large mean EKE areas. This intraseasonal oscillation has a northwestward propagation, with a (phase) speed of ~ 1.0 to 1.5 cm s^{-1} in zonal and meridional velocity. The distribution of mixing parameters in the deep SCS plays a role in both the spatial structure and volume transport of the deep circulation. Deep circulation in the SCS is more sensitive to the large vertical mixing parameters of the Zhongsha Island Chain area than the northern shelf of the SCS and the Luzon Strait. Even though the model is idealized, the model current fields qualitatively reproduce the results of direct current measurement and open new routes to understand the dynamics that mixing regulates the deep circulation. The success of the present model may be associated with several intrinsic features of the deep circulation. It is noteworthy that despite reasonable agreement between the current simulation and observations, surface forcing, which has potential impact on the modification of ocean stratification and the deep circulation (e.g., Su et al. 2014, 2016a, b; Yang 2015), is not applied to the numerical experiments. Although configured with a buffer zone near the eastern boundary, the experiments are currently configured with closed lateral boundary condition, which cannot simulate the interactions between the processes of the current model domain and the Pacific/Indonesia seas. These limitations may introduce uncertainty to some extent to the simulation results in this study. The potential impact of surface forcing and boundary conditions on the deep circulation in the SCS is worth to be investigated.

Authors' contribution All the authors conceived and designed the experiments and contributed ideas in the writing process. X.Z. performed the experiments, analyzed the data, and wrote the paper.

Funding This work was supported by the National Key Research and Development Program of China (Grant no. 2016YFC1402605), the National Natural Science Foundation of China (Grant no. 41806031, 41676011), the Global Change and Air–Sea Interaction Project (Grant no. GASI-IPOVAI-01-03), the National Natural Science Foundation of China (Grant nos. 41606014, 91628302), the Global Change and Air–Sea Interaction Project (Grant no. GASI-IPOVAI-01-02), the East Asia Marine Cooperation Platform (China–ASEAN marine cooperation fund), the National Key Basic Research Program of China (Grant no. 2014CB745003), the Foundation for Innovative Research Groups of the National Natural Science Foundation of China (Grant no. 41521091), and the NSFC–Shandong Joint Fund for Marine Science Research Centers (Grant no. U1406401).

Data availability Model outputs are available upon request to the first author.

References

- Alford MH, MacKinnon JA, Nash JD, Simmons H, Pickering A, Klymak JM, Pinkel R, Sun O, Rainville L, Musgrave R, Beitzel T, Fu K-H, Lu C-W (2011) Energy flux and dissipation in Luzon Strait: two tales of two ridges. *J Phys Oceanogr* 41:2211–2222. <https://doi.org/10.1175/JPO-D-11-073.1>
- Anderson D, Gill A (1975) Spin-up of a stratified ocean, with application to upwelling. *Deep Sea Res Oceanogr Abstr* 22:593–596. [https://doi.org/10.1016/0011-7471\(75\)90046-7](https://doi.org/10.1016/0011-7471(75)90046-7)
- Bleck R (2002) An oceanic general circulation model framed in hybrid isopycnic-Cartesian coordinates. *Ocean Modell* 37:55–88. [https://doi.org/10.1016/S1463-5003\(01\)00012-9](https://doi.org/10.1016/S1463-5003(01)00012-9)
- Cai Z, Gan J (2019) Coupled external-internal dynamics of layered circulation in the South China Sea: a modeling study. *J Geophys Res Oceans* 124:5053. <https://doi.org/10.1029/2019JC014962>
- Cai Z, Gan J, Liu Z, Hui C, Li J (2020) Progress on the formation dynamics of the layered circulation in the South China Sea. *Progr Oceanogr* 181(2020):103346. <https://doi.org/10.1016/j.pocean.2019.102246>
- Carnes MR (2009) Description and evaluation of GDEM-V3.0 Naval Research Laboratory Tech. Rep NRL/MR/7330-09-9165, 21. <https://www7320.nrlssc.navy.mil/pubs/2009/carnes-2009.pdf>. Accessed 2009
- Chang Y-T, Hsu W-L, Tai J-H, Tang T-Y, Chang M-H, Chao S-Y (2010) Cold deep water in the South China Sea. *J Oceanogr* 66:183–190. <https://doi.org/10.1007/s10872-010-0016-x>
- Chao S-Y, Shaw PT, Wu SY (1996) Deep water ventilation in the South China Sea. *Deep-Sea Res I* 43:445–466. [https://doi.org/10.1016/0967-0637\(96\)00025-8](https://doi.org/10.1016/0967-0637(96)00025-8)
- Chassignet EP, Smith LT, Halliwell GR, Bleck R (2003) North Atlantic simulations with the hybrid coordinate ocean model (HYCOM): impact of the vertical coordinate choice, reference pressure, thermobaricity. *J Phys Oceanogr* 33:2504–2526. [https://doi.org/10.1175/1520-0485\(2003\)033<2504:NASWTH>2.0.CO;2](https://doi.org/10.1175/1520-0485(2003)033<2504:NASWTH>2.0.CO;2)
- Chen C-T, Huang MH (1996) A mid-depth front separating the South China Sea Water and the Philippine Sea Water. *J Oceanogr* 52:17–25. <https://doi.org/10.1007/BF02236530>
- Endoh T, Hibiya T (2006) Numerical study of the meridional overturning circulation with “mixing hotspots” in the Pacific Ocean. *J Oceanogr* 62:259–266. <https://doi.org/10.1007/s10872-006-0050-x>
- Ferrari R, Mashayek A, McDougall TJ, Nikurashin M, Campin J-M (2016) Turning ocean mixing upside down. *J Phys Oceanogr* 46:2239–2261. <https://doi.org/10.1175/JPO-D-15-0244.1>
- Forget G, Campin J-M, Heimbach P, Hill CN, Ponte RM, Wunsch C (2015) ECCO version 4: an integrated framework for non-linear inverse modeling and global ocean state estimation. *Geosci Model Dev* 8:3071–3104. <https://doi.org/10.5194/gmd-8-3071-2015>
- Furue R, Endoh M (2005) Effects of the Pacific diapycnal mixing and wind stress on the global and Pacific meridional overturning circulation. *J Phys Oceanogr* 35:1876–1890. <https://doi.org/10.1175/JPO2792.1>
- Gan J, Liu Z, Hui C (2016) A three-layer alternating spinning circulation in the South China Sea. *J Phys Oceanogr* 46:2309–2315. <https://doi.org/10.1175/JPO-D-16-0044.1>
- Gordon AL, Huber BA, Metzger EJ, Susanto RD, Hurlburt HE, Adi TR (2012) South China Sea Throughflow impact on the Indonesian Throughflow. *Geophys Res Lett* 39:L11602. <https://doi.org/10.1029/2012GL052021>
- Hamilton P (2009) Topographic Rossby waves in the Gulf of Mexico. *Progr Oceanogr* 82:1–31. <https://doi.org/10.1016/j.pocean.2009.04.019>
- Jan S, Chern C-S, Wang J, Chao S-Y (2007) Generation of diurnal K1 internal tide in the Luzon Strait and its influence on surface tide in the South China Sea. *J Geophys Res* 112:C06019. <https://doi.org/10.1029/2006JC004003>
- Johns WE, Watts DR (1986) Time scales and structure of topographic Rossby waves and meanders in the deep Gulf Stream. *J Mar Res* 44:267–290. <https://doi.org/10.1357/002224086788405356>
- Kunze E, Firing E, Hummon JM, Chereskin TK, Thurnherr AM (2006) Global abyssal mixing inferred from lowered ADCP shear and CTD strain profiles. *J Phys Oceanogr* 36:1553–1576. <https://doi.org/10.1175/JPO2926.1>
- Lan J, Zhang N, Wang Y (2013) On the dynamics of the South China Sea deep circulation. *J Geophys Res Oceans* 118:1206–1210. <https://doi.org/10.1002/jgrc.20104>
- Lan J, Wang Y, Cui F, Zhang N (2015) Seasonal variation in the South China Sea deep circulation. *J Geophys Res Oceans* 120:1682–1690. <https://doi.org/10.1002/2014JC010413>
- Large WG, McWilliams JC, Doney SC (1994) Ocean vertical mixing: a review and a model with a nonlocal boundary layer parameterization. *Rev Geophys* 32:363–403. <https://doi.org/10.1029/94RG01872>
- Li L, Qu T (2006) Thermohaline circulation in the deep South China Sea basin inferred from oxygen distributions. *J Geophys Res* 111:C05017. <https://doi.org/10.1029/2005JC003164>
- Liu C-T, Liu R-J (1988) The deep current in the Bashi Channel. *Acta Oceanogr Taiwan* 20:107–116
- Mantyla AW (1975) On the potential temperature in the abyssal Pacific Ocean. *J Mar Res* 33:341–353
- McDougall TJ, Ferrari R (2017) Abyssal upwelling and downwelling driven by near-boundary mixing. *J Phys Oceanogr* 47:261–283. <https://doi.org/10.1175/JPO-D-16-0082.1>
- Niwa Y, Hibiya T (2004) Three-dimensional numerical simulation of M2 internal tides in the East China Sea. *J Geophys Res* 109:C04027. <https://doi.org/10.1029/2003JC001923>
- Pickart RS, Watts DR (1990) Deep western boundary current variability at Cape Hatteras. *J Mar Res* 48:765–791. <https://doi.org/10.1357/002224090784988674>
- Platzman GW (1972) Two-dimensional free oscillations in natural basins. *J Phys Oceanogr* 2:117–138. [https://doi.org/10.1175/1520-0485\(1972\)002<0117:TDFOIN>2.0.CO;2](https://doi.org/10.1175/1520-0485(1972)002<0117:TDFOIN>2.0.CO;2)
- Polzin KL, Speer KG, Toole JM, Schmitt RW (1996) Intense mixing of Antarctic bottom water in the equatorial Atlantic Ocean. *Nature* 380(6569):54–57. <https://doi.org/10.1038/380054a0>
- Qu T, Mitsudera H, Yamagata T (2000) Intrusion of the North Pacific waters in the South China Sea. *J Geophys Res* 105:6415–6424. <https://doi.org/10.1029/1999JC900323>
- Qu T, Girton JB, Whitehead JA (2006a) Deepwater overflow through Luzon Strait. *J Geophys Res* 111:C01002. <https://doi.org/10.1029/2005JC003139>
- Qu T, Du Y, Sasaki H (2006b) South China Sea throughflow A heat and freshwater conveyor. *Geophys Res Lett* 33:L23617. <https://doi.org/10.1029/2006GL028350>
- Qu T, Song T, Yamagata T (2009) An introduction to the South China Sea throughflow: its dynamics, variability, implication for climate. *Dyn Atmos Oceans* 47:3–14. <https://doi.org/10.1016/j.dynatmoce.2008.05.001>
- Quan Q, Xue H (2019) Influence of abyssal mixing on the multi-layer circulation in the South China Sea. *J Phys Oceanogr* 49:3045–3060. <https://doi.org/10.1175/JPO-D-19-0020.1>
- Rhines P (1970) Edge-, bottom- and Rossby wave in a rotating stratified fluid. *Geophys Fluid Dyn* 1:273–302. <https://doi.org/10.1080/03091927009365776>

- Shu Y, Xue H, Wang D, Chai F, Xie Q, Yao J, Xiao J (2014) Meridional overturning circulation in the South China Sea envisioned from the high-resolution global reanalysis data GLBa0.08. *J Geophys Res Oceans* 119:3012–3028. <https://doi.org/10.1002/2013JC009583>
- Smith WHF, Sandwell DT (1997) Global seafloor topography from satellite altimetry and ship depth soundings. *Science* 277:1956–1962. <https://doi.org/10.1126/science.277.5334.1956>
- Song YT (2006) Estimation of inter basin transport using ocean bottom pressure: theory and model for Asian marginal seas. *J Geophys Res* 111:C11S19. <https://doi.org/10.1029/2005JC003189>
- Stommel H, Arons AB (1960a) On the abyssal circulation of the world ocean-I stationary planetary flow patterns on a sphere. *Deep-Sea Res* 16:140–154. [https://doi.org/10.1016/0146-6313\(59\)90065-6](https://doi.org/10.1016/0146-6313(59)90065-6)
- Stommel H, Arons AB (1960b) On the abyssal circulation of the world ocean-II an idealized model of the circulation pattern and amplitude in oceanic basins. *Deep-Sea Res* 16:217–233. [https://doi.org/10.1016/0146-6313\(59\)90075-9](https://doi.org/10.1016/0146-6313(59)90075-9)
- Su Z, Ingersoll AP (2016) On the minimum potential energy state and the eddy-size-constrained APE density. *J Phys Oceanogr* 46:2663–2674. <https://doi.org/10.1175/JPO-D-16-0074.1>
- Su Z, Stewart A, Thompson A (2014) An idealized model of Weddell gyre export variability. *J Phys Oceanogr* 44:1671–1688. <https://doi.org/10.1175/JPO-D-13-0263.1>
- Su Z, Ingersoll AP, Stewart AL, Thompson AF (2016a) Ocean convective available potential energy part II: energetics of thermobaric convection and thermobaric cabling. *J Phys Oceanogr* 46:1097–1115. <https://doi.org/10.1175/JPO-D-14-0156.1>
- Su Z, Ingersoll AP, He F (2016b) On the abruptness of Bølling–Allerød warming. *J Clim* 29:4965–4975. <https://doi.org/10.1175/JCLI-D-15-0675.1>
- Su Z, Wang J, Klein P, Thompson AF, Menemenlis D (2018) Ocean submesoscales as a key component of the global heat budget. *Nat Commun* 9(1):775. <https://doi.org/10.1038/s41467-018-02983-w>
- Thompson RORY (1977) Observations of Rossby waves near site D1. *Prog in Oceanogr* 7:1–28. [https://doi.org/10.1016/0079-6611\(77\)90003-9](https://doi.org/10.1016/0079-6611(77)90003-9)
- Tian J, Qu T (2012) Advances in research on the deep South China Sea circulation. *Chin Sci Bull* 57:3115–3120. <https://doi.org/10.1007/s11434-012-5269-x>
- Tian J, Zhou L, Zhang X, Liang X, Zheng Q, Zhao W (2003) Estimates of M2 internal tide energy fluxes along the margin of northwestern Pacific using TOPEX/POSEIDON altimeter data. *Geophys Res Lett* 30:1889. <https://doi.org/10.1029/2003GL018008>
- Tian J, Yang Q, Liang X, Xie L, Hu D, Wang F, Qu T (2006) Observation of Luzon Strait transport. *Geophys Res Lett* 33:L19607. <https://doi.org/10.1029/2006GL026272>
- Tian J, Yang Q, Zhao W (2009) Enhanced diapycnal mixing in the South China Sea. *J Phys Oceanogr* 39:3191–3203. <https://doi.org/10.1175/2009JPO3899.1>
- Wang J (1986) Observation of abyssal flows in the Northern South China Sea. *Acta Oceanogr Taiwan* 16:36–45
- Wang G, Xie S-P, Qu T, Huang RX (2011) Deep South China Sea circulation. *Geophys Res Lett* 38:L05601. <https://doi.org/10.1029/2010GL046626>
- Wang X, Liu Z, Peng S (2017) Impact of tidal mixing on water mass transformation and circulation in the South China Sea. *J Phys Oceanogr* 47:419–432. <https://doi.org/10.1175/JPO-D-16-0171.1>
- Wang D, Wang Q, Cai S, Shang X, Peng S, Shu Y, Xiao J, Xie X, Zhang Z, Liu Z, Lan J, Chen D, Xue H, Wang G, Gan J, Xie X, Zhang R, Chen H, Yang Q (2019) Advances in research of the mid-deep South China Sea circulation. *Sci China Earth Sci* 62:1992–2004. <https://doi.org/10.1007/s11430-019-9546-3>
- Wyrtki K (1961) Physical oceanography of the southeast Asian Waters. The University of California, La Jolla, Scripps Institution of Oceanography
- Xu F, Oey LY (2014) State analysis using the local ensemble transform Kalman filter (LETKF) and the three-layer circulation structure of the Luzon Strait and the South China Sea. *Ocean Dynam* 64:905–923. <https://doi.org/10.1007/s10236-014-0720-y>
- Xu Y, Rolph WD, Mark W, Jae-Hun P (2007) Fundamental-mode basin oscillations in the Japan/east sea. *Geophys Res Lett* 34(4):545–559. <https://doi.org/10.1029/2006gl028755>
- Xu X, Rhines PB, Chassignet EP (2018) On mapping the diapycnal water mass transformation of the upper North Atlantic Ocean. *J Phys Oceanogr* 48:2233–2258. <https://doi.org/10.1175/JPO-D-17-0223.1>
- Yang J (2015) Local and remote wind stress forcing of the seasonal variability of the Atlantic Meridional Overturning Circulation (AMOC) transport at 26.5° N. *J Geophys Res Oceans* 120(4):2488–2503. <https://doi.org/10.1002/2014JC010317>
- Yang Q, Tian J, Zhao W (2010) Observation of Luzon Strait transport in summer 2007. *Deep-Sea Res* 57:670–676. <https://doi.org/10.1016/j.dsr.2010.02.004>
- Yang Q, Tian J, Zhao W (2011) Observation of material fluxes through the Luzon Strait. *Chin J Oceanol Limnol* 29:26–32. <https://doi.org/10.1007/s00343-011-9952-6>
- Yang Q, Zhao W, Liang X, Tian J (2016) Three-dimensional distribution of turbulent mixing in the South China Sea. *J Phys Oceanogr* 46:769–788. <https://doi.org/10.1175/JPO-D-14-0220.1>
- Yaremchuk M, McCreary JJ, Yu Z, Furue R (2009) The South China Sea throughflow retrieved from climatological data. *J Phys Oceanogr* 39:753–767. <https://doi.org/10.1175/2008JPO3955.1>
- Ye R, Zhou C, Zhao W, Tian J, Yang Q, Huang X, Zhang Z, Zhao X (2019) Variability in the deep overflow through the Heng-Chun Ridge of the Luzon Strait. *J Phys Oceanogr* 49:811–825. <https://doi.org/10.1175/JPO-D-18-0113.1>
- Yu X, Naveira Garabato AC, Martin AP, Buckingham CE, Brannigan L, Su Z (2019) An annual cycle of submesoscale vertical flow and restratification in the upper ocean. *J Phys Oceanogr* 49:1439–1461. <https://doi.org/10.1175/JPO-D-18-0253.1>
- Zhang Z, Zhao W, Tian J, Yang Q, Qu T (2015) Spatial structure and temporal variability of the zonal flow in the Luzon Strait. *J Geophys Res* 120:759–776. <https://doi.org/10.1002/2014JC010308>
- Zhao W, Zhou C, Tian J, Yang Q, Wang B, Xie L, Qu T (2014) Deep water circulation in the Luzon Strait. *J Geophys Res* 119:790–804. <https://doi.org/10.1002/2013JC009587>
- Zhao X, Zhou C, Zhao W, Tian J, Xu X (2016) Deepwater overflow observed by three bottom-anchored moorings in the Bashi Channel. *Deep-Sea Res* 110:65–74. <https://doi.org/10.1016/j.dsr.2016.01.007>
- Zhou C, Zhao W, Tian J, Yang Q, Qu T (2014) Variability of the deep-water overflow in the Luzon Strait. *J Phys Oceanogr* 44:2972–2986. <https://doi.org/10.1175/JPO-D-14-0113.1>
- Zhou C, Zhao W, Tian J, Zhao X, Zhu Y, Yang Q, Qu T (2017) Deep western boundary current in the South China Sea. *Sci Rep* 7:9303. <https://doi.org/10.1038/s41598-017-09436-2>
- Zhou C, Zhao W, Tian J, Yang Q, Huang X, Zhang Z, Qu T (2018) Observations of deep current at the Western boundary of the northern Philippine Basin. *Sci Rep* 8:14334. <https://doi.org/10.1038/s41598-018-32541-9>
- Zhu Y, Sun J, Wang Y, Li S, Xu T, Wei Z, Qu T (2019) Overview of the multi-layer circulation in the South China Sea. *Progr Oceanogr* 175:171–182. <https://doi.org/10.1016/j.pocan.2019.04.001>